IEEE Access
Multidisciplinary | Rapid Review | Open Access Journal

Received 9 February 2024, accepted 14 February 2024, date of publication 21 February 2024, date of current version 1 March 2024.

Digital Object Identifier 10.1109/ACCESS.2024.3368051

RESEARCH ARTICLE

Research on Dispersion Compensation of FD-OCT System via Pix2Pix GAN Technique

EDDY WIJANTO[1], HSU-CHIH CHENG[2], BO-HONG LIAO[2], CHUN-MING HUANG[3], AND YAO-TANG CHANG[4]

[1]Department of Electrical Engineering, Universitas Kristen Krida Wacana, Jakarta 11470, Indonesia
[2]Department of Electro-Optical Engineering, National Formosa University, Yunlin 63208, Taiwan
[3]Department of Electronic Engineering, National Formosa University, Yunlin 63208, Taiwan
[4]Department of Information Technology, Kao Yuan University, Kaohsiung 82151, Taiwan

Corresponding author: Chun-Ming Huang (huangcm@nfu.edu.tw)

This work was supported by NSTC under Grant 112-2221-E-150-011 and Grant 112-2221-E-150-028.

ABSTRACT Dispersion in optical coherence tomography (OCT) poses a challenge that is exacerbated by the increased spectral bandwidth, which leads to image blur and feature loss. In this paper, we present a straightforward and cost-effective approach for dispersion compensation in OCT. To achieve this, we employed a pixel-to-pixel (Pix2Pix) generative adversarial network (GAN) architecture customized for image-to-image translation. Two data groups with varying amounts of training image data and epochs were used. The Pix2Pix GAN was trained to generate clear OCT images from the corresponding dispersion-affected OCT images in paired datasets. According to the experimental results, the Pix2Pix GAN technique demonstrated a substantial improvement over the basic GAN. Specifically, it increases the peak signal-to-noise ratio (PSNR) by 159%, structural similarity index (SSIM) by 370%, and Fréchet inception distance (FID) by 274%. These outcomes indicate that the proposed model can generate images with resilience and effectiveness, particularly when dealing with dispersion-affected OCT data.

INDEX TERMS Generative adversarial network, optical coherence tomography, Pix2Pix.

I. INTRODUCTION

Optical coherence tomography (OCT) is a noninvasive imaging method that performs high-resolution cross-sectional imaging. It can produce cross-sectional images of tissue features at the micron scale both in situ and in real time. The basic idea behind OCT is to use low-coherence interferometry (LCI) technology to quantify the path length distribution of scattered or reflected light from an object using a coherence gate [1]. One benefit of OCT is that it can be integrated into a variety of medical devices and implemented using small fiber optic components. According to Fujimoto et al. [2], OCT reduces excisional biopsy sample errors. OCT is a state-of-the-art imaging technique for medical diagnostics that does not require tissue sample removal for microscopic examination. OCT can generate in situ and real-time tissue images by analyzing the interference signals reflected from the reference and sample ends of low-coherence light with high bandwidth and power. Compared to other medical modalities such as computed tomography (CT) and magnetic resonance imaging (MRI), the resolution of OCT is noticeably higher. It has a lateral resolution similar to that of a confocal scanning laser ophthalmoscope, and an axial resolution similar to that of a confocal microscope. Time-domain optical coherence tomography (TD-OCT) and frequency-domain optical coherence tomography (FD-OCT) are two types of OCT system architectures. TD-OCT takes advantage of a low-contrast light source and scan reference delay. A laser source, typically a low-coherence superluminescence diode (SLD) or pulsed laser, is divided into two channels using an optical splitter. A reference mirror moved by the transmission motion bounces light back from the first path, allowing it to travel a known path length and encounter a changeable measurable delay. When the light traveling along the second path is aimed at the sample, the internal structure of the sample scatters the light back, creating interference patterns with the reference light traveling along the same optical channel. This allows for the determination of the depth of the sample and the locations of the different structures within it. In contrast to TD-OCT measurements, in which light

The associate editor coordinating the review of this manuscript and approving it for publication was Jiachen Yang.

echoes are sequentially detected by the step-movement of a reference mirror, FD-OCT measurements detect light echoes as modulations in the source spectrum, with all spectral components being recorded simultaneously. The primary distinction between these two technologies is that, unlike the TD-OCT system, the reference arm of the FD-OCT system features a static mirror. FD-OCT systems may be able to collect data more quickly than TD-OCT systems because of the elimination of mechanical translation.

In biomedical applications, FD-OCT has become a groundbreaking imaging method that provides high-resolution, noninvasive biological tissue visualization. Despite its great success, dispersion remains a major obstacle to realizing the full potential of FD-OCT. Dispersion causes a wavelength-dependent phase shift in the obtained OCT signals and is caused by the wavelength-dependent refractive index of biological tissues. The reconstructed images become distorted because of this occurrence, which affects both the clarity of the images and the precision of tissue characterization. Phase distortion and color separation are caused by the dispersion effect, which occurs when light interacts with biological tissues. Different wavelengths travel at different speeds. Dispersion plays a crucial role in FD-OCT because it builds images through the interference of light waves, thereby influencing the accuracy and integrity of the collected data. This difficulty is particularly noticeable in situations where maximizing the longitudinal resolution of imaging is required.

The fine trade-off between minimizing the negative effects of dispersion and attaining a high longitudinal resolution is at the center of the technical gap in dispersion compensation for FD-OCT. One common technique for improving the longitudinal resolution of FD-OCT is to employ low-coherence light sources. However, this method accentuates the dispersion effect, resulting in blurry images and the loss of important details. The quest for novel and efficient dispersion correction techniques that can harmonize these competing needs has been sparked by the tradeoff between resolution and dispersion.

Dispersion adjustment in FD-OCT is currently achieved mostly through intricate algorithms and calibration processes. Dispersion effects can be mitigated using conventional techniques, such as spectrum shaping and numerical algorithms. Using inverse transforms, numerical algorithms seek to computationally correct the distortions caused by dispersion. Using spectral shaping techniques, the dispersion effects are offset by adjusting the spectral characteristics of the light source. However, these approaches exhibit several drawbacks. In real-world situations, it can be difficult to obtain precise prior information on the sample properties, which is a requirement for many numerical algorithms. Furthermore, their performances may be limited under dynamic imaging conditions or with variable tissue characteristics. Although somewhat successful, spectral shaping techniques can be difficult to use and may not be sufficiently flexible for the variety of tissue features found in biomedical imaging.

The shortcomings of the dispersion correction techniques currently used highlight the need for more durable and flexible solutions to improve the dependability and adaptability of FD-OCT imaging. The search for better techniques is not only an academic endeavor; it is essential to realizing the full promise of FD-OCT in clinical and research applications. Owing to the dynamic nature of in vivo imaging and the intrinsic complexity of biological tissues, compensation approaches must be able to adjust to changing situations effectively without compromising accuracy.

The capacity of machine learning paradigms to handle challenging issues in image synthesis and analysis has made them well-known in recent years. Generative adversarial networks (GANs) are remarkably effective in this context. A particular GAN family architecture, pixel-to-pixel (Pix2Pix), has demonstrated promise for image-to-image translation applications. Pix2Pix offers an innovative solution that uses deep learning to address dispersion-related issues in FD-OCT and dispersion compensation. Pix2Pix operates based on the principle of learning a mapping function between the input and output image pairs in a supervised manner. In FD-OCT, the output images show optimally compensated versions of the scans, whereas the input images show scans distorted by dispersion. Pix2Pix's conditioning feature makes it possible to produce realistic images, making it particularly suitable for the complex process of dispersion correction.

There are various benefits to using Pix2Pix for dispersion adjustment in FD-OCT. First, Pix2Pix can comprehend the complex link between compensated and distributed images by learning intricate mappings from paired datasets. To handle the changing nature of tissue characteristics and imaging situations experienced in practice, adaptability is essential. In contrast to conventional techniques that may not work well in dynamic settings, Pix2Pix can dynamically modify the parameters it has learned, thereby offering real-time correction of distortions caused by dispersion. Second, Pix2Pix's conditional structure enables the creation of images with the required properties. This is particularly helpful in FD-OCT, where it is crucial to preserve important features and precisely depict tissue structures. Another factor in the overall improvement of image quality is Pix2Pix's capacity to produce images with improved clarity while maintaining significant detail.

The intrinsic difficulties caused by dispersion and the potential of machine learning to handle difficult image-translation problems are the driving forces behind the use of the Pix2Pix GAN for dispersion compensation in FD-OCT. Dispersion is a major obstacle in FD-OCT, a potent imaging method with many applications in biomedicine. This can seriously impair image quality and jeopardize the precision of tissue characterization. Pix2Pix GAN's special strengths in the field of image-to-image translation makes it an attractive solution to this problem. A few main factors justify the adoption of the Pix2Pix GAN for dispersion compensation in FD-OCT.

- Adaptability to complex relationships: The basis of Pix2Pix operation is the supervised learning of intricate mappings between pairs of input and output images. The link between compensated and dispersed images in the context of FD-OCT dispersion compensation is complex and dynamic, and changes depending on the imaging settings and tissue characteristics. Owing to its flexibility, Pix2Pix can identify and comprehend intricate linkages, providing a solid foundation for dispersion compensation.
- Conditional image generation: Pix2Pix's conditional feature is especially helpful for FD-OCT dispersion adjustment. This allows the network to create tailored visuals meeting specific requirements. For tasks requiring precision in maintaining details and faithfully representing tissue architecture, Pix2Pix's conditional image generation proves especially beneficial.
- Versatility across tissue types: The dispersion effect varies depending on the characteristics of the biological tissues and how they interact with light. Pix2Pix adapts well to many tissue types because it can learn from various datasets. This flexibility is essential for dispersion correction techniques to be applicable in real-world situations, where tissue characteristics may differ significantly.
- Real-time compensation: Pix2Pix's machine learning-based approach enables real-time adaptation to changing imaging settings. Unlike conventional techniques struggling with quick adjustments, Pix2Pix dynamically modifies learned parameters, providing swift and flexible dispersion compensation. This real-time capability is particularly valuable in time-sensitive clinical situations.
- Possibility for generalization: Pix2Pix has demonstrated efficacy in experimental environments; however, one of its primary driving forces is its potential application in various OCT systems and imaging modalities. Subsequent investigation and advancements may concentrate on verifying and refining the Pix2Pix model to enhance its generalizability, ensuring its efficacy in various biomedical imaging scenarios.

In this study, a Pix2Pix GAN was implemented for dispersion compensation of FD-OCT. The main contributions of this study are as follows.

- Pix2Pix GAN is implemented in the medical imaging domain, which demonstrates its superiority in various areas.
- The method has the feature of simple implementation, effectiveness, and robustness.
- Two data groups of different sizes were used to verify the effect of the training dataset size on the ability of the model to produce high-quality images.
- This study provided and observed qualitative and quantitative results to validate the proposed method.

The remainder of this paper is organized as follows. Section II presents the existing literature and related works in the fields of OCT and GAN to provide a contextual background, highlighting prior research, methodologies, and advancements in both OCT imaging and GAN-based techniques. Section III outlines the theoretical foundations and experimental setup for applying the Pix2Pix GAN technique to address dispersion in FD-OCT, including the Pix2Pix architecture. It also describes in detail how the network is structured to learn and generate compensated images from dispersed OCT scans, the composition of the training datasets, parameters used in training the Pix2Pix model, and any modifications made to adapt the technique to FD-OCT dispersion compensation. Section IV presents the outcomes of the experiments conducted to validate the efficacy of the Pix2Pix GAN in compensating for dispersion in FD-OCT, with qualitative and quantitative comparative analyses with basic GAN methods. Section V concludes the paper by summarizing the key findings of the study.

II. RELATED WORKS

In OCT, even though professionals are trained, there are still some artifacts when scanning samples [3]. When the critical characteristics of a sample structure are obscured by these aberrations, it can be difficult for doctors to examine the images. The phase-shift technique is frequently used to achieve a full-range FD-OCT for artifact reduction. For the suppression of complex conjugate artifacts, Lin et al. [4] presented a five-frame variable phase shift algorithm (FVP) spectral domain optical coherence tomography (SD-OCT). The well-known five-frame invariant phase shift approach is inferior to the FVP method. Additionally, a higher complex conjugate artifact (CCA) suppression rate can considerably enhance the quality of the OCT images. Bao et al. [5] presented a sophisticated technique based on a real spectral phase shift that achieved extremely good artifact reduction. This algorithm provides the highest suppression ratios of all currently used sophisticated artifact suppression techniques, making it suitable for fast, highly precise, and extremely long-range dimensional measurements. Orthogonal polarization with phase-shifting algorithms was suggested by Cheng et al. [6] for use in FD-OCT to increase the image scanning speed and withstand vibrations and other environmental disturbances. By doubling the measurement area, this technique generates sample reconstruction parameters comparable to those obtained from conventional time-domain OCT in one-shot and full-range measurements.

Deep learning (DL), a subset of machine learning techniques, provides solutions to several challenging artificial intelligence (AI)-related issues. The DL model comprises several layers, each of which is connected to its lower and upper levels by different weights. The capacity of DL models to learn feature hierarchies from many forms of data opens up the possibility of tackling a wide range of issues, including those related to medical imaging. Using undersampled spectral data and a DL-based image reconstruction framework, Zhang et al. [7] suggested a method for producing swept-source OCT (SS-OCT) images free of spatial aliasing artifacts. This DL-enabled approach to image reconstruction

can be used with several types of SD-OCT systems to speed up imaging without compromising the image quality or signal-to-noise ratio. Rahul et al. [8] suggested a DL-based approach to classify 347 scans from 134 superficial capillary plexus images of patients using the ResNet152 neural network classifier. In both low- and high-quality images, the results from [8] demonstrated outstanding area under the curve (AUC) metrics. Ahmed et al. [9] introduced a centralized unsupervised DL denoising framework for OCT images, and their experimental findings demonstrated that the system could efficiently reduce speckle noise and provide images with higher quality than existing denoising techniques.

GAN [10] is a method of unsupervised learning. It comprises two neural network models: a generator and a discriminator. By learning through the adversarial relationship between these two networks, a GAN can generate more realistic data from a small amount of data, which is useful for training neural network models. This leads to an improvement in the overall performance of the AI system.

Over time, the GAN architecture has evolved significantly, leading to improved training and generation qualities. The progressive growing of GANs (PGGANs) is another architectural innovation that progressively increases the resolution of images generated during training. PGGANs' superior image quality and stability over conventional GANs enable the production of high-resolution images [11]. Because GANs are adversarial networks, they are inherently unstable, which makes training difficult. Numerous methods have been implemented to address this problem and enhance the training stability. By introducing a new loss function based on the Wasserstein distance, the Wasserstein GAN (WGAN) and its variations stand out in their ability to generate images of higher quality and maintain more stable training dynamics than conventional GANs [12]. Another approach involves controlling the Lipschitz constant of the discriminator using regularization techniques such as weight clipping and spectral normalization. Employing these strategies aids in stabilizing the training process and preventing mode collapse, where the generator struggles to capture the full diversity of the target distribution.

GANs have been effectively used in a number of fields such as text production, video production, picture synthesis, and music composition. Recent developments have focused on creating domain-specific GAN models to satisfy the difficulties and demands of various application domains. For example, text-to-image synthesis GANs (T2I GANs) were designed to produce realistic images based on textual descriptions [13]. These models bridge the gap between text and image modalities by utilizing deep learning and natural language processing techniques. GANs have been used in music generation to produce original compositions and music in various genres. Alternatives, such as WaveGANs and musical instrument digital interface (MIDI) GANs, have demonstrated encouraging results in producing realistic and varied musical compositions [14].

Cao et al. [15] developed a DL method to create high-resolution (HR) OCT images from low-optical and low-digital-resolution (L2R) data. The superresolution GAN (SR-GAN) architecture was designed to accommodate the unique traits of the OCT images better, such as their high structural similarity and textural consistency. The results showed promising visual quality and quantitative performance improvements compared to existing methods. In [16], SiameseGAN, a deep generative model, was used to denoise low signal-to-noise ratio (LSNR) B-scans from SD-OCT. It demonstrated that speckle noise can be quickly and effectively reduced using the proposed method. Bayhaqi et al. [17] used OCT to monitor the smart laser osteotomy ablation process, while DL with a GAN was used to reduce noise. The outcomes demonstrated the potential of DL techniques as a preprocessing stage for tissue classification in laser osteotomy. Taj et al. [18] presented a novel approach for generating more realistic OCT images by using a dual-discriminator Fourier acquisitive GAN (DDFA-GAN). Two discriminators are used by the DDFA-GAN to assess the quality of the generated images. The model considers both the spatial and spectral properties of the images because one discriminator works in the spatial domain and the other works in the Fourier domain. Consequently, the DDFA-GAN can generate images that are more precise and realistic, and can be employed in clinical examinations of the retina, improving the accuracy of the following measures.

The development of conditional GANs (cGANs), which enable controlled generation by conditioning the model on additional data, is a noteworthy breakthrough. cGANs are useful for image-to-image translation tasks, such as translating images from one domain to another or creating realistic images from sketches. Isola et al. [19] proposed a cGAN called Pix2Pix. It is a variation of the GAN in which the input image serves as a condition for the generator network to produce the output image. Pix2Pix performs well in various image-to-image translational tasks. For instance, a Pix2Pix GAN is adept at generating realistic images corresponding to a given input image, making it a valuable tool for image-to-image translation applications. This involves transferring images across domains while preserving the essential structures. Pix2Pix GAN has proven to be a successful tool for completing various image-translation tasks, including turning sketches into realistic images, converting black and white images to colors, and turning daytime images into nighttime images. Owing to its versatility, it can be used in various computer vision, graphics, and creative applications [19]. Its ability to produce visually appealing and high-quality images is further enhanced by conditioning the generator with additional data to ensure that the generated images match the desired output characteristics. This leads to better image quality compared with traditional GANs. To address the common training instability in GANs, Pix2Pix GAN introduces a conditional framework that stabilizes the training process and enables more efficient training of the generator and discriminator networks. The

conditioning information contributed to a more predictable and consistent training phase. Moreover, it provides an easy-to-use interface that enables interactive manipulation of the generated outputs, allowing users to input the desired conditions and promptly observe the results. This feature has contributed significantly to the widespread popularity of Pix2Pix GAN among researchers, designers, and artists engaged in image generation and manipulation.

Dispersion in OCT leads to wavelength-dependent phase distortions that result in poor axial resolution. In practice, all-depth dispersion suppression is challenging, particularly for irregularly structured samples and high-speed processing. Liu et al. [20] proposed an approach to measure dispersion in the fractional Fourier domain (FRFD) and a new dispersion correction technique based on the FRFD stepped detection algorithm, which is capable of adaptively compensating for dispersion at all depths of the sample. The results show that the proposed algorithm for biotissue dispersion correction is practical. A computational method for performing dispersion compensation in FD-OCT and detecting dispersion mismatches was proposed in [21]. The experimental findings demonstrated the applicability of the proposed method for the identification and correction of dispersion mismatches in FD-OCT. Both spectral-domain and swept-source OCT systems can benefit from a robust calibration approach to simultaneously determine the correction vectors for nonlinear wavenumber sampling and dispersion compensation in OCT [22]. Another experimental approach for the estimation and compensation of dispersion in an OCT system was presented in [23]. Dispersion compensation was achieved using the method suggested in [23], and the axial resolution in air increased from 10.6 to 1.9 m. In [24], we proposed using a Pix2Pix GAN as a solution to eliminate artifact noise in FD-OCT images. Artifact noise, which includes conjugate, direct current (DC), and autocorrelation noise, has a significant impact on the accuracy of FD-OCT imaging. As demonstrated by simulation results in [24], the proposed model was designed to translate images with added Gaussian noise into artifact-free FD-OCT depth profiles, successfully eliminating the effect of artifact noise, as demonstrated by simulation results. Furthermore, the Pix2Pix GAN incorporates a loss function that integrates the adversarial loss with the pixel-wise loss. While adversarial loss compels the generator to produce outputs resembling real OCT images, pixel-wise loss guarantees an exact alignment between the generated and target images at the pixel level [25].

III. THEORETICAL AND EXPERIMENTAL SETUP

In the FD-OCT system, an SLD is used as the primary light source. A coupler divides the light into two paths, one of which enters the reference arm, and the other enters the sample arm. The sample to be measured is placed at the sample end and the two light paths are directed towards the reference and sample mirrors, creating interference upon return. The interference light is introduced into an optical spectrum analyzer (OSA), and its optical information is analyzed. Finally, an inverse fast Fourier transform of the interference pattern yields the depth information of the sample. The basic structure of FD-OCT is shown in Fig. 1.

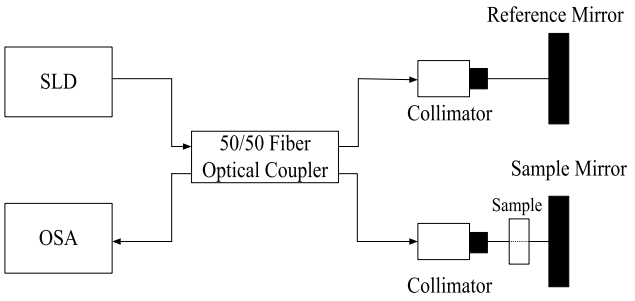

FIGURE 1. Basic FD-OCT architecture.

The sample signal obtained through OSA is as follows:

$$
\begin{aligned}
I_D(\omega) &\propto |S_D(\omega)|^2 \\
&= \left| \int_{-\infty}^{\infty} E_D(t) e^{-i\omega t} dt \right|^2 \\
&= \left| \int_{-\infty}^{\infty} [E_{si}(t-\tau_i) + E_R(t-\tau_R)] e^{-i\omega t} dt \right|^2 \\
&= \left| \sum_{i=0}^{N} S_{si}(\omega) e^{-i\omega\tau_i} + S_R(\omega) e^{-i\omega\tau_R} \right|^2 \\
&= \sum_{i=0}^{N} S_{si0}^2 e^{\frac{-4\ln 2(\omega-\omega_0)^2}{\Delta\omega^2}} + S_{R0}^2 e^{\frac{-4\ln 2(\omega-\omega_0)^2}{\Delta\omega^2}} \\
&\quad + \sum_{i=0}^{N} 2 S_{si0} S_{R0} e^{\frac{-4\ln 2(\omega-\omega_0)^2}{\Delta\omega^2}} \cos[\omega(\tau_j - \tau_i)] \\
&\quad + \sum_{i=0}^{N} 2 S_{si0} S_{R0} e^{\frac{-4\ln 2(\omega-\omega_0)^2}{\Delta\omega^2}} \cos[\omega(\tau_R - \tau_i)] \qquad (1)
\end{aligned}
$$

where I_D is the received photocurrent magnitude, E_D is the received spectrum, S_D is the received photoelectric field intensity, $\tau_i = 2(l_{si} - l_{s0})/c$ is the time delay caused by the optical path difference from the i^{th} layer interface to the sample surface, $\tau_R = 2(l_R - l_{s0})/c$ is the time delay caused by the optical path difference of the light source from the beam splitter to the surface of the sample end and the reference end.

According to (1), the interfering light is composed of four components that result in a pattern of constructive and destructive interference. The first term is the signal reflected through the sample end and the second term is the signal reflected from the beam through the reference end. The third term describes the interference signal generated by each layer of the multilayer structure, if the measured sample is a multilayer structure. The last term refers to the interference between the reference end and the interface of the sample end.

A. DATASET

In this study, a compact OCT system, Lumedica OQ LabScope, was used as the scanning tool. The experimental

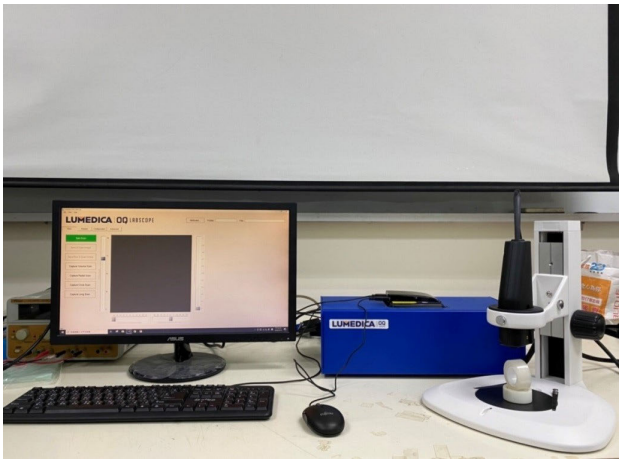

FIGURE 2. Experimental setup of Lumedica OQ LabScope.

setup is illustrated in Fig. 2. This system is designed specifically for high-resolution imaging of biological tissues, utilizing an SLD with a wavelength of 840 nm as its light source, emitting near-infrared light with an output power of 750 μW. The coherence length of this SLD adequately supports the interferometric measurements in OCT. Within the Lumedica OQ LabScope, scanning is executed employing various mechanisms tailored to its specific configuration. These mechanisms enable rapid and precise traversal of the light beam across the sample, ensuring meticulous imaging of the sample.

To generate optical depth information from the sample, the SLD is combined with an interferometer and a high-resolution spectrometer. The light source is split into two beams by a splitter, with one beam directed to the sample arm and the other to the reference arm. Within the sample arm, light is reflected back with sample information by the reflective mirror. This reflected light is then combined with light from the reference arm, resulting in interference that is detected by the spectrometer. The interface between the sample and the OCT system may vary depending on the specific application. Interference occurs at the spectrometer when light returns from both the reference arm and the sample arm, generating a pattern containing depth information about structures within the sample. Ultimately, optical depth images of the sample are computed using a computer, and the resulting OCT data is displayed in real-time, providing high-resolution cross-sectional images of the sample.

Using this system, we generate a dataset of 500 paired image for training purposes. First, the Lumedica OQ LabScope scanned a clear tape image without dispersion. To simulate practical scenarios, the dispersion factor was varied randomly to produce a corresponding tape image affected by dispersion. The two images were then paired and included in the dataset. The two images shown in Fig. 3 were captured using a Lumedica OQ LabScope. Fig. 3(a) shows a tape image with dispersion and Fig. 3(b) shows a clear tape image without dispersion. For conciseness, these two types of scanned OCT images are referred to as dispersion-affected and clear OCT images in the remainder of this paper. Dispersion decreases the sensitivity and image quality of the FD-OCT system.

B. IMPLEMENTATION SETUP

We suggest using a Pix2Pix GAN with FD-OCT systems to simply and inexpensively reconstruct dispersion-affected OCT images. The Pix2Pix GAN [26] is a cGAN model composed of a generator and discriminator. The main difference between cGANs and regular GANs is that the former uses additional information to guide the generation process, allowing the generator to be trained to produce samples with specific attributes or characteristics. Therefore, a dataset comprising pairs of dispersion-affected and clear OCT images was used to train the GAN model. Specifically, the generator model was trained to learn the mapping from the input dispersion-affected OCT image to a corresponding clear OCT image, which is referred to as the generated image. In addition, a discriminator model was trained to distinguish the generated image from a real, clear OCT image. Using this approach, the system was able to improve the quality of the FD-OCT images. Fig. 4 illustrates the functioning of a cGAN through a block diagram. The central element in this process is the random noise vector, represented as Z. This noise serves as a crucial input for the generator in a GAN. Introducing stochasticity ensures that the generator produces diverse outputs under the same input conditions. Additionally, fake labels, denoted as y_{fake}, are introduced to provide the generator with supplemental conditional information. These labels guide the generation process in the cGAN, enabling the generator to produce samples with specific features or characteristics.

By utilizing Z and y_{fake} as inputs, the generator generates x_{fake}, representing the artificially created data. The primary objective of the generator is to craft data that closely resembles actual samples by combining conditional information and random noise. On the other hand, the real input data is represented as x_{real}, such as actual images from a dataset that the GAN aims to enhance or imitate. The corresponding genuine labels that match the real input data are denoted as y_{real}.

In the cGAN framework, real input samples are paired with labels, and the discriminator learns from these pairs. The discriminator takes x_{real} and y_{real}, as well as x_{fake} and y_{fake}, as inputs. Its role is to distinguish between real and generated images by evaluating the authenticity of input data and labels. The ultimate output of the cGAN system is represented as y, with its interpretation varying according to the specific task of the cGAN. For instance, in an image-to-image translation task, y may denote the generated output, expected to closely resemble the real input data.

During the training process, the generator strives to generate fake data (x_{fake}) that closely mirrors the real data (x_{real}) by leveraging conditional information (y_{fake}) and random noise (Z). Simultaneously, the discriminator is trained with x_{fake} and x_{real}, along with their corresponding labels, i.e. y_{fake} and y_{real}, to effectively distinguish between real and

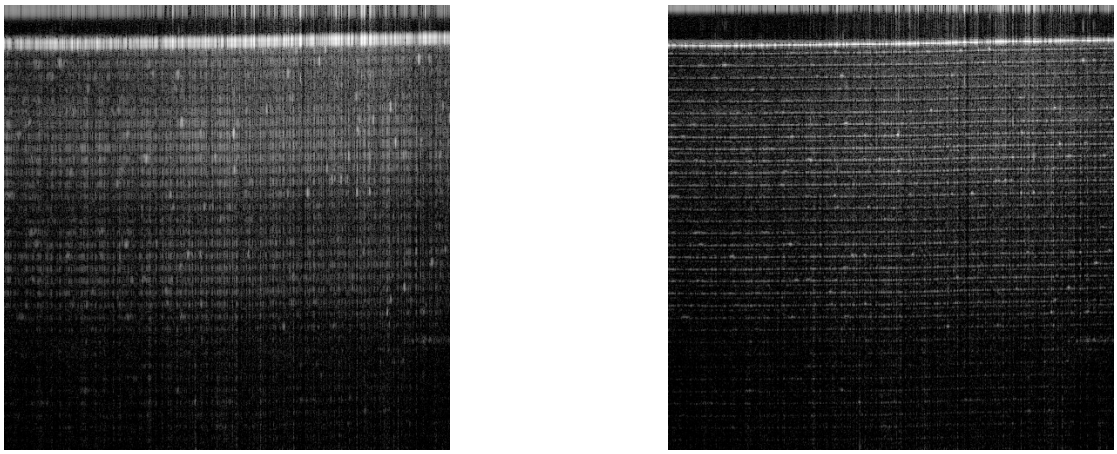

FIGURE 3. Depth image with dimensions of 600 pixels wide and 600 pixels high. (a) Source image with severe dispersion. (b) Clear target image.

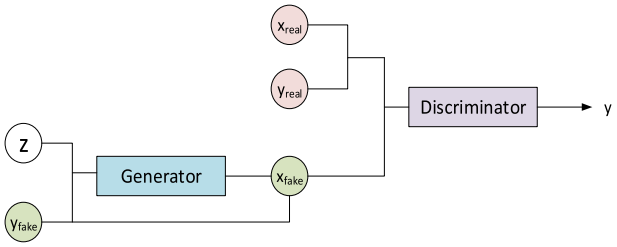

FIGURE 4. Block diagram of conditional GAN.

generated data. As training progresses, the discriminator enhances its accuracy in making distinctions, leading to an improvement in the generator's capacity to generate realistic outputs through the adversarial interplay between the two components.

The generator creates target images that are comparable to the source image using an encoder-decoder model and U-Net architecture. Fig. 5 depicts the architecture of the convolutional neural network used in this study. The sizes of the feature maps learned by the convolutional layers are indicated in red and the number of channels in each layer is denoted in black. The encoder on the left side of the U-Net architecture extracts important information from the input image, whereas the decoder on the right side reconstructs this information to generate target image. A skip connection is added between the symmetrical positions on both sides to prevent information loss. Pix2Pix GAN falls within the cGAN category, meaning that it uses additional information to direct image production during training. These additional data, in the context of Pix2Pix, are pairs of clean and dispersion-affected OCT images. The training dataset comprises two sets of clean OCT images with dispersion issues. Each pair functions as a guide for the cGAN. The model learns to map an OCT image affected by dispersion to its equivalent clean OCT image. There is only one discriminator and generator in the Pix2Pix GAN. The generator captures the source images (dispersion-affected OCT images) and converts them into target images (clean OCT images). The generator adheres to the U-Net architecture and uses an encoder-decoder mechanism. The discriminator is trained to distinguish between real and clear OCT images and generated images. The generator is motivated by this adversarial process to generate images that are identical to real OCT images. The generator is taught to learn the mapping from dispersion-affected to clear images, thereby improving the quality of the FD-OCT images. This process is aided by a discriminator, which provides a generator input to produce more realistic images. The U-Net architecture is adhered to by a Pix2Pix's generator. Convolutional neural networks with a U-Net architecture are well known for their effectiveness in image-segmentation applications.

The encoder is located on the left side of the U-Net design, whereas the decoder is on the right side. From the input dispersion-affected OCT image, the encoder pulls the necessary information that the decoder reconstructs to provide the desired clear OCT image. Skip connections are added to prevent information loss during the encoding-decoding process. The network can maintain fine-grained information owing to these connections, which link symmetrical locations on both sides of the U-Net architecture. The encoder is responsible for obtaining the input image and extracting the pertinent characteristics. Important information regarding dispersion-affected OCT images is probably captured by the encoder in the context of Pix2Pix. To create the desired clear OCT image, the decoder uses the encoded data and reconstructs it. In this rebuilding procedure, skip connections are essential for maintaining details. The generator is trained to produce clear OCT images as the output from dispersion-affected OCT images as the input. The discriminator assesses the produced images in tandem with real OCT images. The generator's capacity to generate high-quality OCT images that are difficult for the discriminator to discern from authentic images is improved through the adversarial training procedure. The primary limitation in the process of noise reduction and image enhancement is the kernel size;

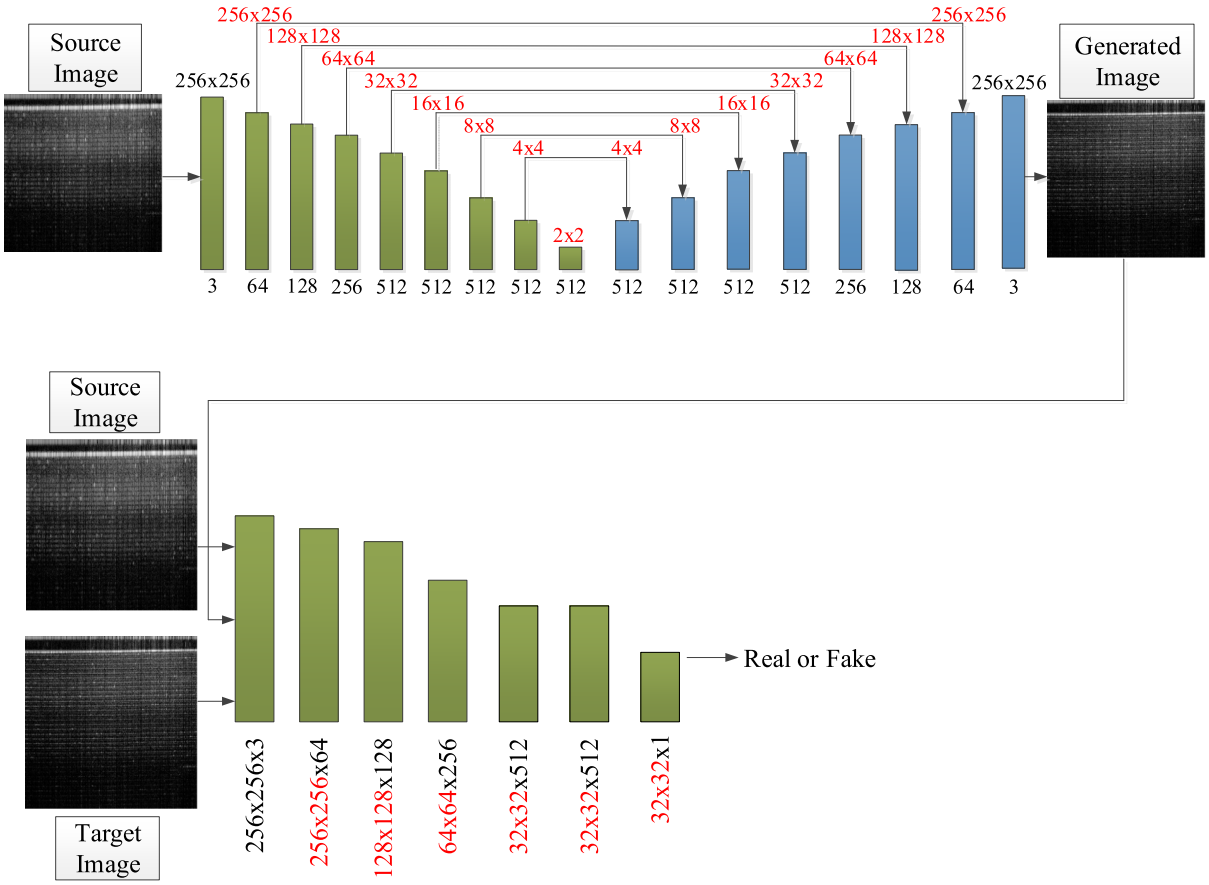

FIGURE 5. FD-OCT image enhancement system using Pix2Pix GAN technique.

thus, considerable attention must be paid when selecting the kernel [27]. All convolutional layers in the network used a stride of 2 and a kernel size of 4 × 4. Because of its relatively modest size, a 4 × 4 kernel enables the model to identify local features in the input image. Furthermore, the model is computationally more efficient because smaller kernel sizes typically result in fewer parameters. Using a 4 × 4 kernel achieves a compromise between considering global information and capturing local features because Pix2Pix GANs are designed to transform an input image into a corresponding output image. This design choice enables the network to learn complex features from the input images and effectively perform image enhancement.

Adversarial loss and *L1* loss, which calculate the differences between the generated and expected target images, are used to optimize the generator during training. The generator model is designed to produce an accurate translation of the source image using this additional loss. The objective of the proposed model is as follows [28]:

$$L_{GAN}(G, D) = E_{x,y}[\log D(x, y)] + E_x[\log(1 - D(x, G(x)))] \tag{2}$$

where x is the original image, y is the corresponding target image set to the ground truth of x, and $L_{GAN}(G,D)$ is the adversarial loss between the generator and discriminator. To increase its adversarial discriminator D, the generator G attempts to reduce this aim with the following optimized outcome:

$$G^* = \arg\min_G \max_D L_{GAN}(G, D) \tag{3}$$

where G^* is the optimized generator.

The *L1* losses of the generated and expected target images can be assessed using the following criteria:

$$L1\,(G) = E_{x,y}\left[\|y - G\,(x)\|_1\right] \tag{4}$$

The proposed model final objective can be expressed as follows:

$$G^* = \arg\min_G \max_D L_{GAN}(G, D) + \lambda L1\,(G) \tag{5}$$

The design of the discriminator is based on the PatchGAN model [29]. The output is a matrix each element of which represents a local region of the input image; we get 1 (Real) if the local region is real, and 0 (Fake) otherwise. In this method, the model focuses more on the details owing to the discriminative output through several small blocks of the image. Except for the output layer, which uses a sigmoid function to map the output to the range [0,1], all convolutional layers use a rectified linear unit (ReLU) activation function. To accelerate the convergence and mitigate overfitting, a batch normalization layer is included

after each convolutional layer in the neural network, except for the output layer.

To assess the quality of the generated image and how closely it approximates the corresponding real OCT image, three evaluation metrics were used: the peak signal-to-noise ratio (PSNR), structural similarity index (SSIM), and Fréchet inception distance (FID). These metrics were chosen because they are commonly used to measure the differences between images and provide an accurate estimate of their degree of similarity.

PSNR computes the ratio of the maximum value of the image signal to the noise. Typically, PSNR is converted into decibels (dB) using a logarithmic function, with a higher value indicating a better image quality. PSNR is calculated using the following formula [30]:

$$PSNR = 10\log_{10}\frac{L_{\max}^2}{MSE} \tag{6}$$

where L_{max} is the highest pixel value that may be assigned to an image. Mean squared error (MSE) is the most popular regression loss function, and is the average of the sum of the squares of the differences between the target and generated images. The formula for MSE is as follows:

$$MSE = \frac{1}{N}\sum_{i}^{N}(x-y)^2 \tag{7}$$

where N represents the number of elements in the array. x and y are the target and generated images, respectively.

SSIM measures the similarity between two images. A score between 0 and 1 is provided, with a number closer to 1 indicating a greater similarity between the images. [31]. The primary purpose of the SSIM algorithm is to detect the similarity between two images of the same size, or to measure the degree of image distortion. The SSIM algorithm compares the brightness, contrast, and structure of two images, weights these three elements, and is expressed by the following equation [32]:

$$\begin{aligned} SSIM(x,y) &= [l(x,y)]^{\alpha}[c(x,y)]^{\beta}[s(x,y)]^{\gamma}, \\ l(x,y) &= \frac{2\mu_x\mu_y + C_1}{\mu_x^2 + \mu_y^2 + C_1}, \\ c(x,y) &= \frac{2\sigma_x\sigma_y + C_2}{\sigma_x^2 + \sigma_y^2 + C_2}, \\ s(x,y) &= \frac{\sigma_{xy} + C_3}{\sigma_x\sigma_y + C_3}, \end{aligned} \tag{8}$$

where $l(x, y)$ compares the brightness of x and y; $c(x, y)$ compares the contrast; and $s(x, y)$ compares the structural information. The values of α, β, and γ are positive parameters that can be used to fine-tune the sensitivities of $l(x, y)$, $c(x, y)$, $s(x, y)$. μ_x (or μ_y) and σ_x (or σ_y) represent the average and standard deviation of x (or y), respectively. σ_{xy} denotes the covariance between x and y. C_1, C_2, and C_3 are constants used to ensure the stability of $l(x, y)$, $c(x, y)$, $s(x, y)$, respectively.

For practical use, the formula is typically simplified by setting the parameters $\alpha = \beta = \gamma = 1$ and $C_3 = C_2/2$, resulting in the following equation:

$$SSIM = \frac{(2\mu_x\mu_y + C_1)(2\sigma_{x,y} + C_2)}{(\mu_x^2 + \mu_y^2 + C_1)(\sigma_x^2 + \sigma_y^2 + C_2)} \tag{9}$$

Fréchet inception distance (FID) is a widely employed metric in image generation, particularly within the framework of GANs. It is a quantitative measure used to assess the fidelity of generated images compared with real images. Developed to enhance earlier metrics such as the inception score, FID incorporates statistical and perceptual aspects in its evaluation.

$$\begin{aligned} &FID(x,g) \\ &= \left\|\mu_x - \mu_g\right\|^2 + Tr\left(\sum x + \sum g - 2\left(\sum x \sum g\right)^{1/2}\right) \end{aligned} \tag{10}$$

where μ_x and μ_g are the means, and $\sum x$ and $\sum g$ are the covariance matrices of the real and generated image features, respectively. The term $\left\|\mu_x - \mu_g\right\|^2$ represents the squared Euclidean distance between the means and $Tr\left(\sum x + \sum g - 2\left(\sum x \sum g\right)^{1/2}\right)$ is the trace of the square root of the product of the covariance matrices. A lower FID score indicates better agreement between the real and generated image distributions.

IV. EXPERIMENTAL RESULTS AND DISCUSSION

The proposed GAN-based FD-OCT model for dispersion compensation is presented in this section, along with the experimental findings. The model was developed using Python 3.7 with the Tensorflow library and trained by the RTX 3080Ti. First, we present the results from the basic GAN in Fig. 6, which was trained with 150 epochs for 500 training images with an image size of 600 × 600 pixels. Because basic GANs generate samples from random noise, the generated images are of poor quality. The basic GAN is different from the Pix2Pix GAN, which leverages paired training data consisting of input-output image pairs. This pairing provides explicit supervision during training, enabling the model to learn the specific mapping between the input and output. This supervised learning approach contributes to more stable and reliable training compared with the unsupervised nature of basic GANs. The PSNR, SSIM, and FID values of the images generated with the basic GAN were worse than those of the others.

Two data groups (#1 and #2) of different sizes were prepared for the Pix2Pix experiments. Both groups contained training and validation datasets. In data group#1 (data group#2), the training and validation datasets were generated, and consisted of 250 (500) and 50 image pairs, respectively, with an image size of 600 × 600 pixels. The images in the training dataset were used to train the GAN and the validation dataset was used to verify the effectiveness of the trained network. Using these two datasets allowed us to assess the effect of the size of the training dataset on the ability of the model to produce high-quality images. The translated images

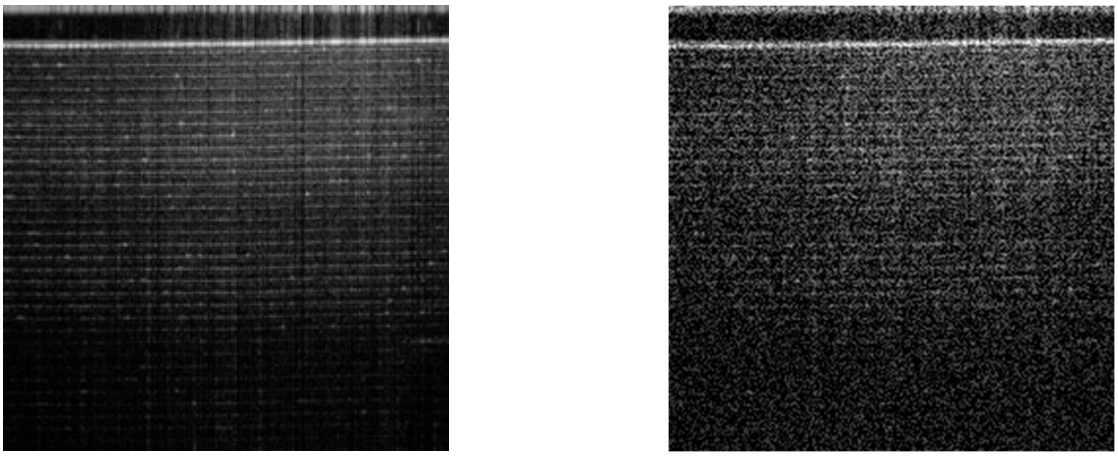

(a) (b)

FIGURE 6. Basic GAN. (a) Clear target image (b) Generated image.

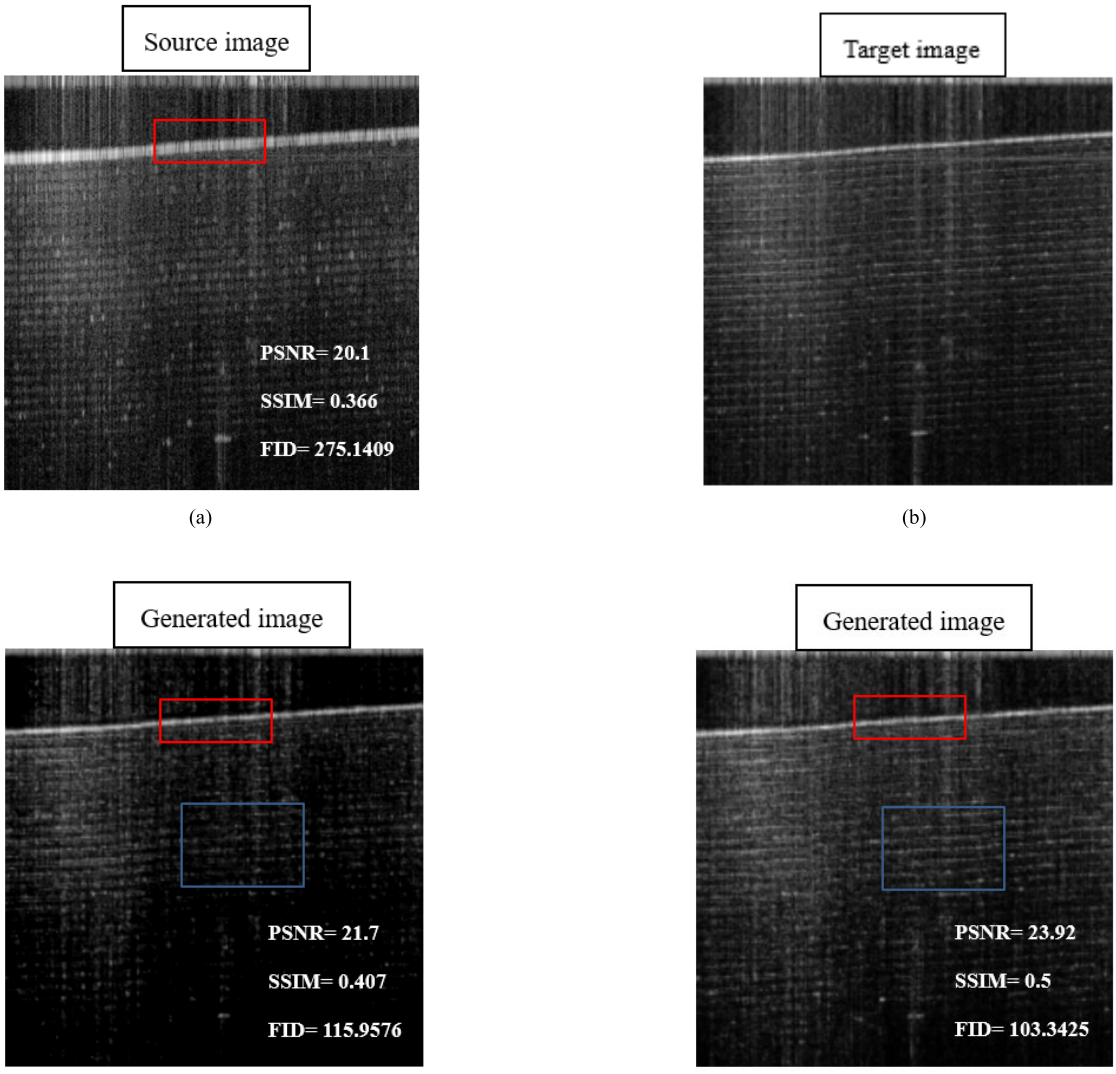

(a) (b) (c) (d)

FIGURE 7. Image generation results of FD-OCT based on Pix2Pix GAN for data group#1. (a) Severely dispersive source image. (b) Target image. (c) Generated image from models trained with epoch 10. (d) Generated image from models trained with epoch 150.

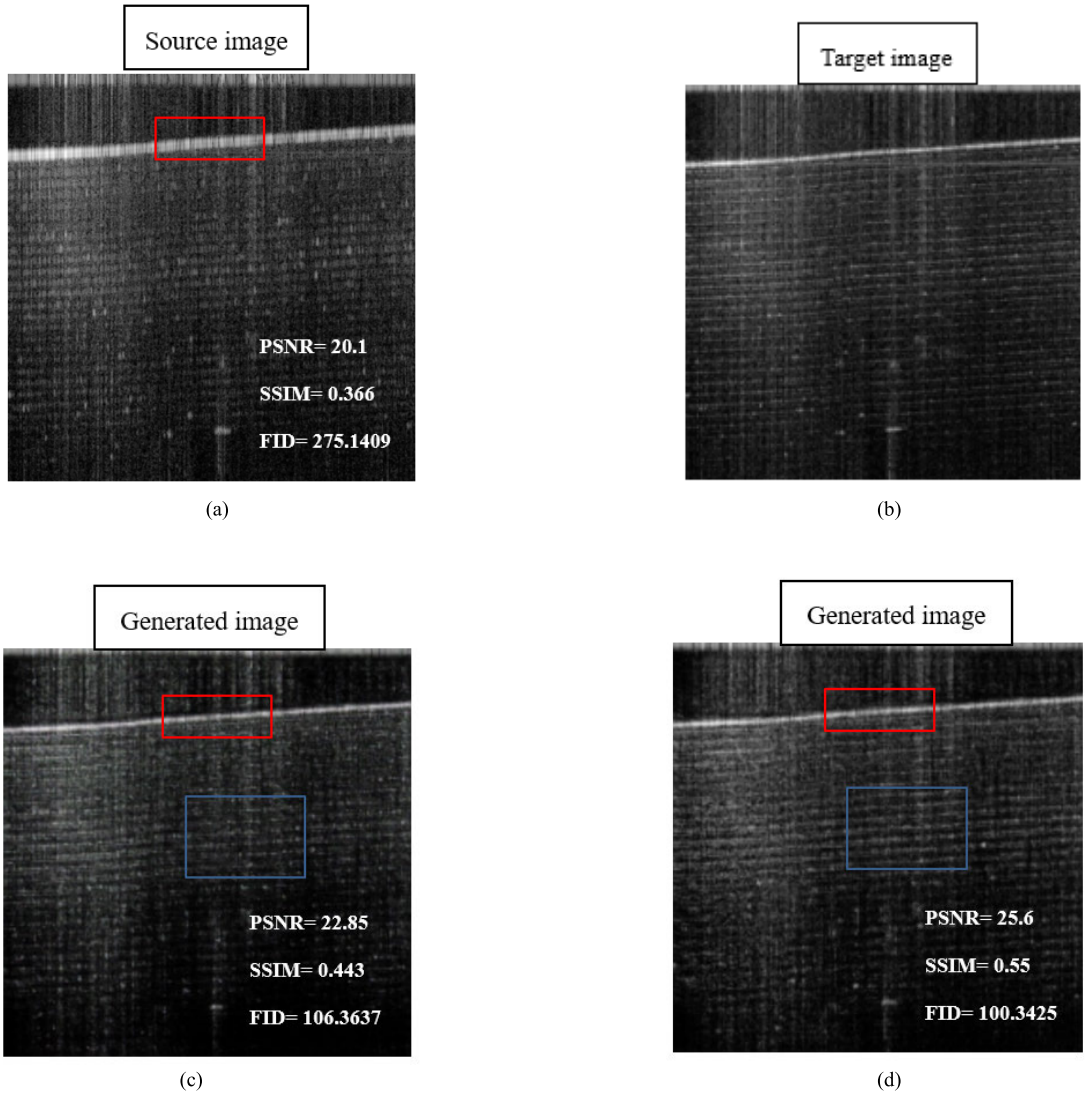

FIGURE 8. Image generation results of FD-OCT based on Pix2Pix GAN for data group#2. (a) Severely dispersive source image. (b) Target image. (c) Generated image from models trained with data group#2 with epoch 10. (d) Generated image from models trained with data group#2 with epoch 150.

produced by the saved model after every 10 epochs were used to observe the results.

A. TRAINING ON DATA GROUP#1

Data group#1 was trained with a smaller number of images to observe the effect of image quantity on dispersion compensation. A dataset of 250 images was input into the GAN for training. Two different number of epochs was implemented to see the image quality. The number of epochs was set to 10 and 150 to compare image quality. For every epoch, the training data were passed through the algorithm, updating the hyperparameters. The results were saved and evaluated after every 10 epochs. In the case with 150 epochs, a total of 15 trained models were saved in H5 format. After training, 50 dispersed images from the validation dataset were randomly selected and input into the trained models to generate a clear image. Fig. 7 presents the results of FD-OCT based on the Pix2Pix GAN trained with data group#1. Fig. 7(a) shows one of the 50 severely dispersed images in the validation dataset. Fig. 7(b) shows the target image. Fig. 7(c) shows a clear image generated by the model trained for 10 epochs. The lines in the blue box are still blurry. In contrast, the model trained for 150 epochs generated a sharper image that is closer to the target image, as shown in Fig. 7(d).

B. TRAINING ON DATA GROUP#2

Further training was conducted for data group#2, which had more images than in data group#1. For training, a dataset of 500 images was input into the GAN. The number of epochs was set to 10 and 150 to compare image quality. After training, 50 dispersed images from the validation dataset were randomly selected and input into the trained models to generate a clear image. Fig. 8 presents the results

TABLE 1. Results of accuracy and similarity quantitative comparison of severely dispersive images and generated images.

	Source Image	Basic GAN Epoch = 150	Data Group#1 Epoch=10	Data Group#1 Epoch= 150	Data Group#2 Epoch= 10	Data Group#2 Epoch= 150
Average PSNR	20.06dB	15.92dB	21.58dB	23.72dB	22.62dB	25.3dB
SSIM	0.364	0.146	0.395	0.48	0.43	0.54
FID	122.9079	275.1409	115.9576	103.3425	106.3637	100.3425

of FD-OCT based on the Pix2Pix GAN trained with data group#2. Fig. 8(a) shows one of the 50 severely dispersed images in the validation dataset. Fig. 8(b) shows the target image. Fig. 8(c) shows a clear image generated by the model trained for 10 epochs. The lines in the blue box are still blurry. In contrast, the model trained for 150 epochs generated a sharper image that is closer to the target image, as shown in Fig. 8(d). The lines in the red box indicate that the resulting image is sharper than the heavily dispersed image.

A summary of the experiment is presented in Table 1, which shows the average quantitative analysis of the image quality generated by the network model trained by data groups#1 and #2 for the 50 images in the validation dataset. The PSNR, SSIM, and FID values of the images generated by the model trained for 150 epochs in data group#2 are significantly better than the others. The number of training epochs and training image affected the generated image. The images produced by the model trained for 10 epochs in data group#2 had poor feature learning ability despite the high number of images and modest number of training cycles. In data group#1, the number of training images was too small; even after training for 150 epochs, the quality of the reconstructed images remained poor.

V. CONCLUSION

This paper proposes a Pix2Pix GAN-based FD-OCT system to enhance image quality, using severely dispersed images and clear images captured by the FD-OCT system based on a Michelson interferometer and Pix2Pix GAN for training.

Two data groups were established to compare whether the number of training images and training sessions affected the quality of the generated images. The experimental results showed that the proposed Pix2Pix GAN-based FD-OCT system successfully generated clear images, and models with a longer training time generated better image quality. We increased the number of images used for training and observed that the image generated by the model with more image data and longer training times was the best.

We showed that the proposed model produced clear images; however, when the amount of image data was too small, the trained model was ineffective. Our proposed Pix2Pix GAN-based FD-OCT benefits from a straightforward design and reasonable computational cost because it does not require complicated algorithms or architectures. Our future research will leverage GAN to analyze intricate FD-OCT depth profile structures. This involves optimizing the network and upgrading hardware scanning tools to enable effective training with a limited amount of image data. Improvements to the pix2pix GAN model include the adoption of techniques such as attention mechanisms, which concentrate on specific regions of interest in OCT images and enhance the model's translation accuracy and resource allocation efficiency. In addition, to capture complex patterns and improve the translation quality, we plan to introduce residual blocks and explore the use of deeper and wider networks.

REFERENCES

[1] P. A. Flournoy, R. W. McClure, and G. Wyntjes, "White-light interferometric thickness gauge," *Appl. Opt.*, vol. 11, no. 9, p. 1907, 1972.

[2] J. G. Fujimoto, C. Pitris, S. A. Boppart, and M. E. Brezinski, "Optical coherence tomography: An emerging technology for biomedical imaging and optical biopsy," *Neoplasia*, vol. 2, nos. 1–2, pp. 9–25, Jan. 2000.

[3] S. Asrani, L. Essaid, B. D. Alder, and C. S. Turla, "Artifacts in spectral domain optical coherence tomography measurements in glaucoma," *JAMA Ophthalmol.*, vol. 132, no. 4, pp. 396–402, 2014.

[4] J. Lin, S. Zhong, Q. Zhang, and W. Chen, "Five-frame variable phase-shifting method for full-range spectral-domain optical coherence tomography," *Appl. Sci.*, vol. 8, no. 9, p. 1580, Sep. 2018.

[5] W. Bao, Y. Shen, T. Chen, P. Li, and Z. Ding, "High-speed high-precision and ultralong-range complex spectral domain dimensional metrology," *Opt. Exp.*, vol. 23, no. 9, p. 11013, 2015.

[6] H. C. Cheng and M. S. Shiu, "Experimental demonstration of high-speed full-range Fourier domain optical coherence tomograpy imaging using orthogonally polarized light and a phase-shifting algorithm," *Appl. Opt.*, vol. 51, pp. 8762–8768, Dec. 2012.

[7] Y. Zhang, T. Liu, M. Singh, E. Çetintaş, Y. Luo, Y. Rivenson, K. V. Larin, and A. Ozcan, "Neural network-based image reconstruction in swept-source optical coherence tomography using undersampled spectral data," *Light, Sci. Appl.*, vol. 10, no. 1, p. 155, Jul. 2021.

[8] R. M. Dhodapkar, E. Li, K. Nwanyanwu, R. Adelman, S. Krishnaswamy, and J. C. Wang, "Deep learning for quality assessment of optical coherence tomography angiography images," *Sci. Rep.*, vol. 12, no. 1, Aug. 2022, Art. no. 13775.

[9] H. Ahmed, Q. Zhang, R. Donnan, and A. Alomainy, "Unsupervised region-based denoising for optical coherence tomography framework," in *Proc. 7th Int. Conf. Comput. Intell. Appl. (ICCIA)*, Jun. 2022, pp. 267–273.

[10] I. Goodfellow, "Generative adversarial networks," in *Proc. Adv. Neural Inf. Process. Syst.*, vol. 3, 2014, pp. 1–9.

[11] M. Hoffmann, L. Malburg, and R. Bergmann, "ProGAN: Toward a framework for process monitoring and flexibility by change via generative adversarial networks," in *Proc. Int. Conf. Bus. Process Manag.*, 2021, pp. 43–55.

[12] M. Arjovsky, "Wasserstein GAN," in *Proc. ICML*, 2017, pp. 214–223.

[13] Y. X. Tan, C. P. Lee, M. Neo, and K. M. Lim, "Text-to-image synthesis with self-supervised learning," *Pattern Recognit. Lett.*, vol. 157, pp. 119–126, May 2022.
[14] S. Shahriar and N. Al Roken, "How can generative adversarial networks impact computer generated art? Insights from poetry to melody conversion," *Int. J. Inf. Manage. Data Insights*, vol. 2, no. 1, Apr. 2022, Art. no. 100066.
[15] S. Cao, X. Yao, N. Koirala, B. Brott, S. Litovsky, Y. Ling, and Y. Gan, "Super-resolution technology to simultaneously improve optical & digital resolution of optical coherence tomography via deep learning," in *Proc. 42nd Annu. Int. Conf. IEEE Eng. Med. Biol. Soc. (EMBC)*, Jul. 2020, pp. 1879–1882.
[16] N. A. Kande, R. Dakhane, A. Dukkipati, and P. K. Yalavarthy, "SiameseGAN: A generative model for denoising of spectral domain optical coherence tomography images," *IEEE Trans. Med. Imag.*, vol. 40, no. 1, pp. 180–192, Jan. 2021.
[17] Y. A. Bayhaqi, A. Hamidi, F. Canbaz, A. A. Navarini, P. C. Cattin, and A. Zam, "Deep-learning-based fast optical coherence tomography (OCT) image denoising for smart laser osteotomy," *IEEE Trans. Med. Imag.*, vol. 41, no. 10, pp. 2615–2628, Oct. 2022.
[18] M. Tajmirriahi, R. Kafieh, Z. Amini, and V. Lakshminarayanan, "A dual-discriminator Fourier acquisitive GAN for generating retinal optical coherence tomography images," *IEEE Trans. Instrum. Meas.*, vol. 71, pp. 1–8, 2022.
[19] P. Isola, J.-Y. Zhu, T. Zhou, and A. A. Efros, "Image-to-image translation with conditional adversarial networks," in *Proc. IEEE Conf. Comput. Vis. Pattern Recognit. (CVPR)*, Jul. 2017, pp. 5967–5976.
[20] D. Liu, C. Ge, Y. Xin, Q. Li, and R. Tao, "Dispersion correction for optical coherence tomography by stepped detection algorithm in fractional Fourier domain," *Opt. Exp.*, vol. 28, no. 5, pp. 5919–5935, 2020.
[21] G. Ni, "Detection and compensation of dispersion mismatch for frequency-domain optical coherence tomography based on A-scan's spectrogram," *Opt. Exp.*, vol. 28, no. 13, pp. 19229–19241, 2020.
[22] X. Attendu and R. M. Ruis, "Simple and robust calibration procedure for k-linearization and dispersion compensation in optical coherence tomography," *J. Biomed. Opt.*, vol. 24, no. 5, p. 1, May 2019.
[23] K. Singh, G. Sharma, and G. J. Tearney, "Estimation and compensation of dispersion for a high-resolution optical coherence tomography system," *J. Opt.*, vol. 20, no. 2, Feb. 2018, Art. no. 025301.
[24] C.-M. Huang, E. Wijanto, and H.-C. Cheng, "Applying a Pix2Pix generative adversarial network to a Fourier-domain optical coherence tomography system for artifact elimination," *IEEE Access*, vol. 9, pp. 103311–103324, 2021.
[25] T. Schlegl, P. Seebock, S. Waldstein, U. Schmidt-Erfurth, and G. Langs, "Unsupervised anomaly detection with generative adversarial networks to guide marker discovery," in *Proc. Int. Conf. Inf. Process. Med. Imag.*, 2017, pp. 146–157.
[26] A. Mino and G. Spanakis, "LoGAN: Generating logos with a generative adversarial neural network conditioned on color," in *Proc. 17th IEEE Int. Conf. Mach. Learn. Appl. (ICMLA)*, Orlando, FL, USA, Dec. 2018, pp. 965–970.
[27] P. N. Srinivasu, V. E. Balas, and N. M. Norwawi, "Performance measurement of various hybridized kernels for noise normalization and enhancement in high-resolution MR images," *Bio-Inspired Neurocomput.*, vol. 2021, pp. 1–24, Jan. 2021.
[28] O. Ronneberger, P. Fischer, and T. Brox, "U-Net: Convolutional networks for biomedical image segmentation," in *Proc. MICCAI*, vol. 9351, 2015, pp. 234–241.
[29] Q. Hao, K. Zhou, J. Yang, Y. Hu, Z. Chai, Y. Ma, G. Liu, Y. Zhao, S. Gao, and J. Liu, "High signal-to-noise ratio reconstruction of low bit-depth optical coherence tomography using deep learning," *J. Biomed. Opt.*, vol. 25, no. 12, Nov. 2020, Art. no. 123702.
[30] U. Demir and G. Unal, "Patch-based image inpainting with generative adversarial networks," 2018, *arXiv:1803.07422*.
[31] A. Horé and D. Ziou, "Image quality metrics: PSNR vs. SSIM," in *Proc. 20th Int. Conf. Pattern Recognit.*, Aug. 2010, pp. 2366–2369.
[32] Z. Wang, A. C. Bovik, H. R. Sheikh, and E. P. Simoncelli, "Image quality assessment: From error visibility to structural similarity," *IEEE Trans. Image Process.*, vol. 13, no. 4, pp. 600–612, Apr. 2004.

EDDY WIJANTO received the B.S. degree from the Department of Electrical Engineering, Universitas Kristen Krida Wacana, Indonesia, in 2005, the M.S. degree from the Department of Electrical Engineering, Pelita Harapan University, Indonesia, in 2009, and the Ph.D. degree from the Electro-Optical Engineering Department, National Formosa University, Yunlin County, Taiwan, in 2021. He is currently an Associate Professor with the Department of Electrical Engineering, Universitas Kristen Krida Wacana. His major research interests include the areas of wireless and optical communications.

HSU-CHIH CHENG received the B.S. degree from the Electronics Department, National Taiwan University of Science and Technology, in 2000, and the M.S. and Ph.D. degrees in electrical engineering from National Cheng Kung University, Tainan, Taiwan, in 2002 and 2006, respectively. He is currently a Full Professor with the Department of Electro-Optical Engineering, National Formosa University, Yunlin County, Taiwan. His major research interests include DWDM networking devices, optical system design, and optics fiber sensor.

BO-HONG LIAO received the M.S. degree from the Institute of Electro-Optical and Materials Science, National Formosa University, Yunlin County, Taiwan. His research interests include the areas of optics fiber sensors and optical communications.

CHUN-MING HUANG received the B.S. degree from the Department of Electrical Engineering, National Cheng Kung University, Tainan, Taiwan, in 2000, and the M.S. and Ph.D. degrees from the Communication and Network Group, Institute of Computer and Communication Engineering, in 2005 and 2009, respectively. From 2010 to 2018, he was an Associate Scientist with the National Chung-Shan Institute of Science and Technology, Longtan, Taiwan. He is currently an Associate Professor with the Department of Electronic Engineering, National Formosa University, Yunlin County, Taiwan. His major research interests include the areas of error control codes and optical communications.

YAO-TANG CHANG received the M.A.Sc. and Ph.D. degrees from the Department of Electrical Engineering, National Cheng Kung University, Taiwan, in 2002 and 2007, respectively. He has been a Professor with the Department of Information Technology, Kao Yuan University, Kaohsiung, Taiwan, since 2008. Formerly, he was the Directorate General of Telecommunications and National Communications Commission for government. His major research interests include the cryptography of reconfigurable optical wired or wireless communications networks.